IEICE TRANSACTIONS

on Fundamentals of Electronics, Communications and Computer Sciences

DOI:10.1587/transfun.2024SMP0008

Publicized:2024/08/27

This advance publication article will be replaced by the finalized version after proofreading.

A PUBLICATION OF THE ENGINEERING SCIENCES SOCIETY

The Institute of Electronics, Information and Communication Engineers

Kikai-Shinko-Kaikan Bldg., 5-8, Shibakoen 3 chome, Minato-ku, TOKYO, 105-0011 JAPAN

PAPER

Frequency-domain weighted FxLMS algorithm for feedback active noise control

Yosuke SUGIURA[†a)], ***Member***, **Ryota NOGUCHI**[†], ***Nonmember***, ***and*** **Tetsuya SHIMAMURA**[†], ***Member***

SUMMARY In this paper, we propose the frequency-domain weighted FxLMS algorithm for feedback active noise control. This algorithm aims to resolve the slow convergence issue of the conventional FxLMS algorithms by integrating a frequency-weighted method. This method dynamically adjusts weights based on the amplitude-frequency characteristics of narrowband noise, thereby improving tracking performance for time-varying narrowband noise. Through simulation experiments, we reveal that the FD-WFxNLMS algorithm achieves fast convergence, outperforming the conventional algorithms in feedback ANC systems.

key words: *active noise control, feedback ANC, filtered-x LMS, frequency-domain adaptive algorithm*

1. Introduction

Active noise control (ANC) is a technique to suppress undesirable noise sounds by emitting sound waves with an opposite phase from a loudspeaker. ANC systems are categorized into three categories: feedforward ANC (FF-ANC), feedback ANC (FB-ANC), and hybrid ANC (HANC). The structure of the feedback ANC system is illustrated in Figure 1. Compared to other ANC systems that require a reference microphone, the architecture of FB-ANC offers a more cost-effective implementation. Due to its feedback configuration, FB-ANC is adept at suppressing narrowband noise emanating from sources such as machine vibrations [1] and aircraft [2]. In this paper, we assume that the secondary path $C(z)$ is accurately modeled. There are various methods [3]-[5] that can be used for this modeling.

In Fig. 1, the control filter $W(z)$ plays a role as a predictor of the narrowband noise. Therefore, it is essential to continuously update the coefficients of $W(z)$ quickly and accurately in accordance with change of the narrowband noise characteristics. While several methods [6], [7] employ non-linear filters like deep neural networks for superior noise suppression, their real-time implementation is challenged by substantial computational complexity. Hence, this paper adopts a linear filter, which offers the benefit of low computational complexity.

The update algorithms for the control filter are typically categorized into three types: filtered-x least-mean-square (FxLMS), filtered-x affine projection (FxAP), and filtered-x recursive least square (FxRLS). The FxLMS algorithm exhibits a simple structure, thus it has been extensively studied and extended. The FxAP algorithm, which is more computationally intensive than FxLMS, achieves a faster convergence. While the FxRLS algorithm exhibits the fastest convergence among them, it is infrequently employed in practical applications due to its high computational complexity. In this paper, our focus lies on the FxLMS algorithm and enhancing its performance.

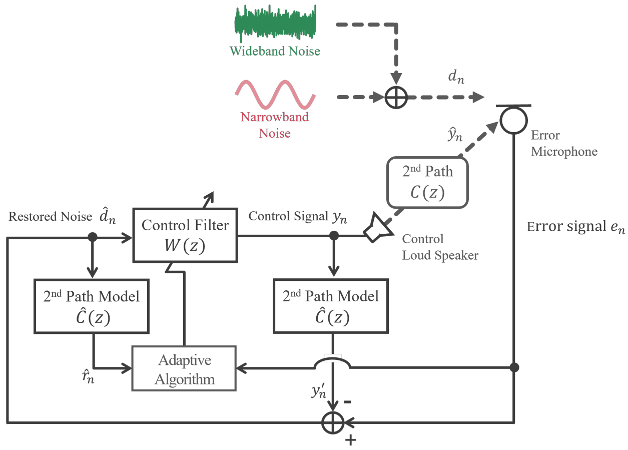

Fig. 1: Structure of general feedback ANC

The FxLMS algorithm used in FB-ANC system has two primary issues. The first one is instability, which is similar to that observed in an adaptive IIR filter. To address this problem, the constrained gain method has been investigated [8]. This method introduces constraints into the gradient of FxLMS to prevent large amplitude variations when the characteristics of the error signal change. However, this leads to the second issue: slow convergence.

The issue of slow convergence remains a fundamental obstacle for the FxLMS algorithm. Although numerous variable step-size (VSS) methods have been developed for FF-ANC and HANC to mitigate this issue [9]-[12], it is a significant challenge in applying most of them to FB-ANC. Among them, Leaky-FxLMS (LFxLMS) [13] especially stands out as one of the effective VSS methods for FB-ANC, which employs a strategy similar to the Leaky-LMS algorithm.

The performance of LFxLMS can be enhanced by appropriately adjusting the leakage factor. A few works [14], [15] provide insights into an optimal leakage factor for frequency-domain LFxLMS, utilizing the frequency characteristics of the narrowband noise component. However, in the practical situations, the effectiveness of the LFxLMS

[†]The author is with the Faculty of Engineering, Saitama University.
a) E-mail: ysugiura@mail.saitama-u.ac.jp

algorithm is limited since the amplitude-frequency characteristics of the narrowband noise is unknown.

To tackle the issue of slow convergence, the proposed method employs a frequency-weighted approach that dynamically adjusts weights of the error signal based on the amplitude-frequency characteristics of the narrowband noise. This method assigns larger weights only to frequencies with higher amplitudes in the narrowband signal. This is similar to the Variable Step Size (VSS) approach [15], which assigns larger step sizes only to frequencies with higher amplitudes in the narrowband signal. Unlike the method in [15], however, our method detects the amplitude of the narrowband signal by identifying its local peaks along the frequency axis using an erosion operator. Therefore, the proposed method has the advantage of achieving faster convergence without requiring any prior information. Additionally, the proposed method introduces the normalized step size [16], enabling further stability and faster convergence.

This approach requires performing the erosion operation, which is a nonlinear process, on the amplitude spectrum. Therefore, it is difficult to implement in the time domain. Before introducing the proposed VSS, it is essential to first derive the frequency-domain block FxLMS (FD-FxLMS) algorithm that employs FFT. Although the FD-FxLMS algorithm with FFT has been established for FF-ANC [17], its application to FB-ANC remains unexplored, except for FD-FxLMS using DFT [14], wavelet transform [18], [19], or subband filter [20]. Subsequently, the proposed method is meticulously derived and validated through the simulation experiments.

2. Frecuency-domain Block FxLMS algorithm for feedback ANC

In this section, we formulate the FD-FxLMS algorithm for FB-ANC. Figure 2 shows the structure of feedback ANC using FD-FxLMS. In this figure, d_n is noise at time n, modeled as

$$d_n = u_n + s_n, \tag{1}$$

where u_n is broadband noise, and s_n is narrowband noise. Let $\hat{y}$ represent the control signal that reaches the error microphone through the secondary path, $\hat{y}$ is represented by:

$$\hat{y}_n = \sum_{k=0}^{M-1} c_k y_{n-k}, \tag{2}$$

where the sequence $[c_0, c_1, \cdots, c_{M-1}] = \boldsymbol{c}$ denotes the impulse response of the secondary path with a length of M. Using $\hat{y}_n$, we can express the error signal detected by the error microphone as:

$$e_n = d_n + \hat{y}_n. \tag{3}$$

With $\boldsymbol{w}^n = \left[w_0^n, w_1^n, \cdots, w_{M-1}^n\right]$ representing the coefficient vector of length N at time n, the control signal y_n is calculated as follows:

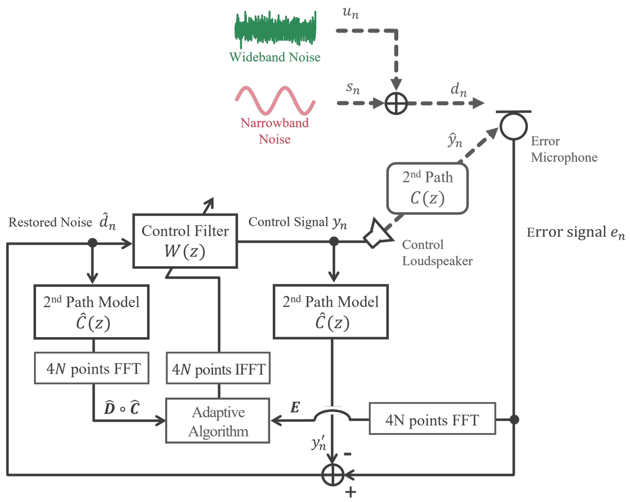

Fig. 2: Structure of feedback ANC with frequency-domain block FxLMS (FD-FxLMS) algorithm.

$$y_n = \sum_{k=0}^{M-1} w_k^n \hat{d}_{n-k}, \tag{4}$$

where $\hat{d}_n$ is the reconstructed noise signal, which is derived by:

$$\hat{d}_n = e_n - \sum_{k=0}^{L-1} \hat{c}_k y_{n-k}. \tag{5}$$

It is assumed that the secondary path $\boldsymbol{c}$ has been previously estimated. The model of the secondary path is denoted as $\hat{\boldsymbol{c}}$, with its length defined as L.

Next, we introduce the FD-FxLMS algorithm that incorporates FFT. To simplify the calculation of the FFT, N is set as 2^k in this paper. Initially, we compute the frequency response of $\hat{\boldsymbol{c}}$ with a length of $4N$ as follows:

$$\hat{\boldsymbol{C}} = \text{FFT}\left(\left[\hat{c}_L, \hat{c}_{L-1}, ..., \hat{c}_1, \boldsymbol{0}^{1\times(4N-L)}\right]\right) \tag{6}$$

The FD-FxLMS for w_k^n at time n is defined by:

$$\hat{\boldsymbol{d}} = \left[\boldsymbol{0}^{1\times N}, \hat{d}_{n-3N+1}, \hat{d}_{n-3N+2}, ..., \hat{d}_n\right], \tag{7}$$

$$\hat{\boldsymbol{D}} = \text{FFT}(\hat{\boldsymbol{d}}), \tag{8}$$

$$\boldsymbol{Z} = \hat{\boldsymbol{D}} \circ \hat{\boldsymbol{C}}, \tag{9}$$

$$\boldsymbol{e} = \left[e_{n-N+1}, e_{n-N+2}, ..., e_n, \boldsymbol{0}^{1\times 3N}\right], \tag{10}$$

$$\boldsymbol{E} = \text{FFT}(\boldsymbol{e}), \tag{11}$$

$$\boldsymbol{g} = N \cdot \text{IFFT}(\boldsymbol{Z} \circ \boldsymbol{E}), \tag{12}$$

$$\boldsymbol{w}^{i+1} = \boldsymbol{w}^i - \hat{\mu}\left[\boldsymbol{I}^{N\times M}, \boldsymbol{0}^{N\times 4N-M}\right] \boldsymbol{g}^T, \tag{13}$$

where $\boldsymbol{0}$ is a zero matrix, $\boldsymbol{I}$ is an identity matrix which has 1 on the diagonal elements and 0 elsewhere, $\circ$ is an operator of Hadamard product, and μ is a step-size parameter which is chosen within the range (0,1) for stability. It is important to note that while the FD-FxLMS algorithm for feedforward ANC requires $2N$-points FFT/IFFT [17], this algorithm utilizes $4N$-points FFT/IFFT. It is important to note that while the conventional FD-FxLMS algorithm for feedforward ANC requires $2N$-points FFT/IFFT [17], this algorithm utilizes $4N$-points FFT/IFFT. The rationale for this requirement is explained in Appendix B.

The FD-FxLMS algorithm updates the coefficients every K samples. Hence, to ensure the same performance across the TD-FxLMS and FD-FxLMS algorithms, the step-size parameter of the FD-FxLMS needs to be scaled by K relative to the step-size parameter of the FD-FxLMS algorithm, μ. Namely, $\hat{\mu}$ is adjusted as follows:

$$\hat{\mu} = K\mu. \tag{14}$$

The normalized version of FD-FxLMS, that is called FD-FxNLMS, is easily derived by defining $\hat{\mu}$ by:

$$\hat{\mu} = \frac{K\mu}{\frac{N}{3N}\sum_{i=0}^{3N-1}\hat{d}_{n-i}^2}, \tag{15}$$

where the term $N/3N$ in the denominator serves to scale the power of $\hat{\boldsymbol{d}}$ across $3N$ samples down to N samples. The FD-FxNLMS algorithm using Eq. (15) demonstrates the same convergence performance as the TD-FxNLMS algorithm.

Both the TD-FxLMS and the FD-FxLMS algorithms for feedback ANC, despite being the normalized versions, encounter a fundamental issue of slow convergence, especially when the narrowband noise is buried in the broadband noise.

3. Frequency-domain Weighted Block FxLMS (FD-WFxLMS) algorithm for FB-ANC

To enhance the performance of narrowband noise suppression, we incorporate the frequency-weighted technique into the FD-FxLMS algorithm for FB-ANC. Specifically, the proposed method assigns weights to $\boldsymbol{E}$ which is the frequency response of the error signal in Eq. (11). These weights are adjusted based on the amplitude ratio between the error signal and the broadband noise included in it.

The amplitude ratio can be roughly estimated by using the erosion operation to E_k, which is the k-th frequency components of the error signal. The definition of the erosion operation for $|E_k|$ is given as:

$$\Phi(|E_k|, l) = \min\left([|E_{k-l}|, |E_{k-l+1}|, \cdots, |E_{k+l}|]\right), \tag{16}$$

where l is a frame length for the erosion operation. The erosion operation $\Phi(|E_k|, l)$ removes the positive peaks in $|\boldsymbol{E}|$. With the assumption that the narrowband noise is modeled by line spectra, $\Phi(|E_k|, l)$ approximates the spectral envelope of the broadband noise. Hence, the amplitude ratio can be calculated by:

$$R_k = \frac{|E_k|}{\Phi\left(|E_k|, l\right)}. \tag{17}$$

Furthermore, by taking the logarithm of both sides, the following equation is derived:

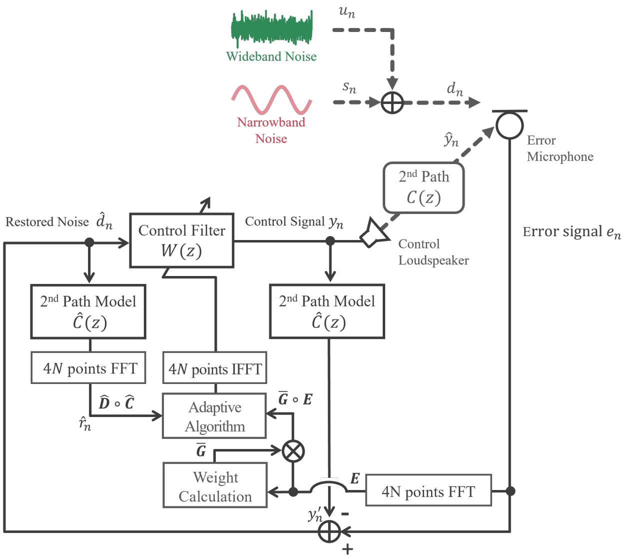

Fig. 3: Structure of feedback ANC with frequency-domain block weighted FxLMS (FD-WFxLMS) algorithm.

$$\begin{aligned}\log_{10} R_k &= \log_{10}\frac{|E_k|}{\Phi\left(|E_k|, l\right)}\\ &= \log_{10}|E_k| - \log_{10}\Phi\left(|E_k|, l\right)\\ &= \log_{10}|E_k| - \Phi\left(\log_{10}|E_k|, l\right)\end{aligned} \tag{18}$$

The transformation from the second equation to the third equation is provided in Appendix A. It is clear that the ratio $\log_{10} R_k$ increases as the power of the narrowband noise rises. Focusing on this property, the proposed method assigns a large weight for the k-th frequency bin where $\log_{10} R_k$ exhibits high values.

Figure 3 shows the structure of feedback ANC with FD-WFxLMS algorithm. The FD-WFxLMS algorithm calculates the frequency response of the weighted error signal, $\hat{\boldsymbol{E}}$, and then replace $\boldsymbol{E}$ by it in Eq. (11). The calculation procedure of $\hat{\boldsymbol{E}}$ in the Fx-WFxLMS algorithm is as follows:

$$\bar{E}_k^i = \gamma\bar{E}_k^{i-1} + (1-\gamma)\left|E_k^i\right|, \tag{19}$$

$$\bar{A}_k = \log_{10}\left(\bar{E}_k^i + \epsilon\right) - \log_{10}\epsilon, \tag{20}$$

$$\bar{R}_k = \bar{A}_k - \Phi(\bar{A}_k, l), \tag{21}$$

$$\alpha_n = \beta\sum_{k=1}^{4N}\bar{R}_k, \tag{22}$$

$$G_k = \alpha_n\bar{R}_k + 1, \tag{23}$$

$$\bar{G}_k = \begin{cases}\alpha_{\max} & , G_k \geq \alpha_{\max}\\ G_k & , G_k < \alpha_{\max}\end{cases}, \tag{24}$$

$$\hat{\boldsymbol{E}} = \bar{\boldsymbol{G}} \circ \boldsymbol{E}, \tag{25}$$

where γ is a smoothing factor satisfying $0 < \gamma < 1$, ϵ is a small positive value, and β is a positive scaling factor. In Eqs. (19) and (20), averaging and logarithmic transformation are applied to E_k to mitigate the effects of fluctuations in $\boldsymbol{E}$. In Eq. (23), the weight G_k is adjusted using the power of the narrowband noise calculated in Eq. (22). The weight

$\bar{G}_k$ becomes larger as the power of the narrowband noise increases, but it approaches 1 as the narrowband noise is effectively suppressed. For stability, G_k is saturated at the upper limit of $\alpha_{\max}$.

The normalized version of FD-WFxLMS, that is FD-WFxNLMS, is also available when the step-size parameter is determined by Eq. (15).

4. Computational Complexity

The computational complexity of the FD-FxLMS algorithm for FB-ANC can be calculated by counting the number of real multiplications required for the following operations:

- In Eqs. (8), (11) and (12), 3 times of $4N$-points FFT/IFFT require $3 \times 4N \log_2(4N) = 12N \log_2(4N)$ multiplications. The average computational complexity per sample is given by $12N \log_2(4N)/K$.
- In Eqs. (9) and (12), 2 times of Hadamard product operations require $3 \times [2 \times 4N] = 24N$ multiplications, where the 3 outside the square brackets corresponds to the complex filtering.The average computational complexity per sample is given by $24N/K$.
- The calculation of Eq. (13) requires M multiplications, since $\left[\boldsymbol{I}^{N\times M}, \boldsymbol{0}^{N\times 4N-M}\right] \boldsymbol{g}^T$ can be implemented by slicing $\boldsymbol{g}^T$ within the index range of $(1, M)$. The average computational complexity per sample is given by M/K.
- In the control filter, M multiplications per sample are required to obtain y_n.

The FD-WFxLMS algorithm requires the following additional costs:

- In Eq. (19), $2 \times 4N/K = 8N/K$ multiplications per sample are required.
- In Eq. (23), $4N/K$ multiplications per sample are required.
- In Eq. (25), $3 \times 4N/K = 12N/K$ multiplications are required for the complex Hadamard product operation.

Table 1 summarizes the average computational complexity of each algorithm, including the operations of multiplication (Mul), addition (Add), division (Div), absolute value (Abs), logarithm (Log), and minimum (Min). Figure 4 illustrates Weighted Million Operations Per Second (WMOPS) [21] versus frame length N with $L = 128$, $K = M = N$, and $l = 7$. According to Ref. [21], the weights assigned to each operator are defined as follows: Mul (3), Add (1), Div (32), Abs (1), Log (5), and Min(1). Here, the logarithmic function is approximated by a piecewise linear function using a lookup table. Under these conditions, the frequency-domain algorithms exhibit lower computational complexity than the time-domain algorithms, owing to the utilization of FFT instead of convolution operations. Focusing on $N = 512$, the FD-WFxLMS algorithm reduces WMOPS by 41.1% compared to the TD-FxLMS algorithm, and the FD-WFxNLMS algorithm reduces WMOPS by 55.8% compared to the TD-FxNLMS algorithm.

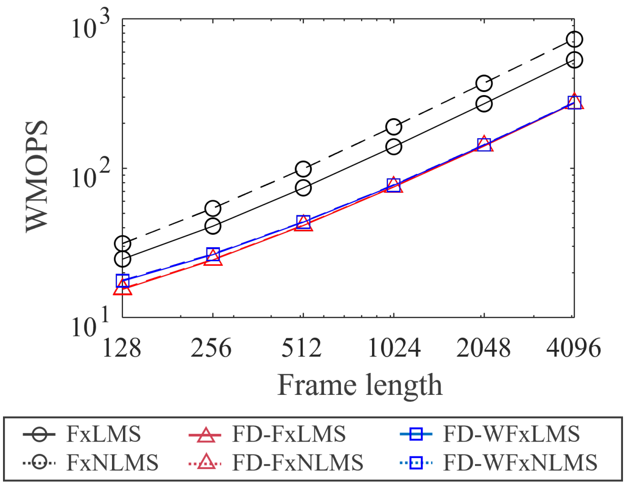

Fig. 4: WMOPS versus frame length N for each algorithm with $L = 128$, $K = M = N$, and $l = 7$.

5. Simulation Experiments

To evaluate the effectiveness of the FD-WFxNLMS algorithm, simulation experiments of FB-ANC were conducted. In the experiments, TD-FxNLMS, TD-LFxNLMS, and FD-FxNLMS algorithms were used for comparison. The unnormalized series, such as TD-FxLMS, were excluded from this experiments, due to their significantly slower convergence speeds.

As a metric for performance evaluation, we employ Averaged Noise Reduction (ANR) [22], which is calculated using the following equation:

$$\mathrm{ANR}_n = 20 \log_{10} \frac{A_e(n)}{A_d(n)}, \tag{26}$$
$$A_e(n) = \kappa A_e(n-1) + (1-\kappa)|e_n|, \tag{27}$$
$$A_d(n) = \kappa A_d(n-1) + (1-\kappa)|d_n|. \tag{28}$$

In the experiment, we set $A_e(0) = 0$, $A_d(0) = 0$, $\kappa = 0.999$.

The secondary path is obtained in a real environment, as illustrated in Figure 5. In this setup, the control loudspeaker is positioned 20 cm away from the error microphone in the anechoic room. Figure 6 depicts the frequency response of the obtained secondary path $\boldsymbol{C}$. As shown in the figure, the amplitude spectrum has no notches and the phase spectrum remains linear, except at the DC and the Nyquist frequencies. This indicates that noise can be effectively controlled across the entire frequency band, except in the regions around the DC and Nyquist frequencies. For simplicity, we have assumed that the estimated secondary path model $\hat{\boldsymbol{C}}$ is the same as $\boldsymbol{C}$. We employed two types of noise: synthetic noise and real noise for performance evaluation.

The parameter settings that we used are the followings: the sampling frequency F_S is set to 16 kHz, $M = N = K = 256$, $\mu = 0.005$, $l = 7$, $\beta = 0.005$, $\gamma = 0.8$, $\alpha_{\max} = 20$, $\epsilon = 10^{-20}$.

Table 1: Average computational complexity of each algorithm.

Algorithm	Muls	Adds	Divs	Abs	Logs	Mins
FxLMS	$2M+L+1$	$2M+L-2$	0	0	0	0
FxNLMS	$3M+L+1$	$3M+L-3$	1	0	0	0
FD-FxLMS	$\frac{12N\log_2(4N)+24N+M}{K}+M$	$\frac{24N\log_2(4N)+M}{K}+M-1$	0	0	0	0
FD-FxNLMS	$\frac{12N\log_2(4N)+27N+M}{K}+M$	$\frac{24N\log_2(4N)+3N+M-1}{K}+M-1$	$\frac{1}{K}$	0	0	0
FD-WFxLMS	$\frac{12N\log_2(4N)+48N+M}{K}+M$	$\frac{24N\log_2(4N)+20N+M-1}{K}+M-1$	0	$\frac{4N}{K}$	$\frac{4N}{K}$	$\frac{4NI}{K}$
FD-WFxNLMS	$\frac{12N\log_2(4N)+51N+M}{K}+M$	$\frac{24N\log_2(4N)+23N+M-2}{K}+M-1$	$\frac{1}{K}$	$\frac{4N}{K}$	$\frac{4N}{K}$	$\frac{4NI}{K}$

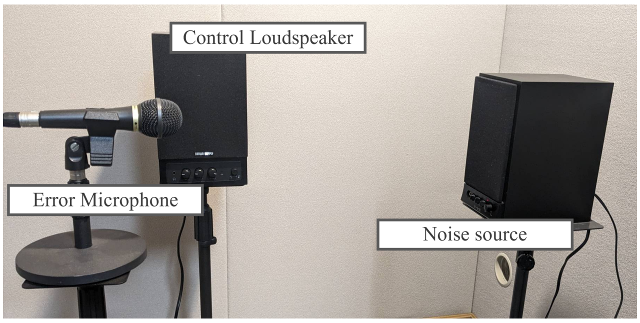

Fig. 5: Experimental environment for determining the secondary path.

5.1 Case I: Active noise control using synthetic noise

In the first experiment, we conducted an active noise control simulation using synthetic noise to assess convergence performance. The broadband noise used in this experiment, u_n, is generated by filtering white Gaussian noise using a 2nd-order IIR filter. The frequency characteristics of this filter are modeled after factory floor noise [23], which is similar to pink noise, a common type of colored noise. The transfer function of the filter is as follows:

$$H(z) = 1 - 1.2\cos(0.01\pi j)z^{-1} + 0.36z^{-2}. \tag{29}$$

The narrowband noise is defined as follows:

$$s_n = \sum_{i=1}^{4} \sin(k\omega_n n), \tag{30}$$

where the frequencies $k\omega_n$ are aligned with the spectrogram depicted in Figure 7. The broadband noise and narrowband noise are mixed with $\log_{10}\left(\sum s_n^2 / \sum u_n^2\right) = 10\,[\text{dB}]$.

In the FD-WFxNLMS algorithm, α_n is a crucial parameter, which is directly influencing the magnitude of the weight $\bar{\boldsymbol{G}}$. Figure 8 displays the transient behavior of α_n. This figure shows that α_n decreases when narrowband noise is suppressed, notably between 0.0 s and 2.5 s, and between 5.0 s and 7.5 s. Conversely, α_n increases quickly with changes in the narrowband noise characteristics. This behavior indicates that α_n effectively serves as a suitable weight for the error signal.

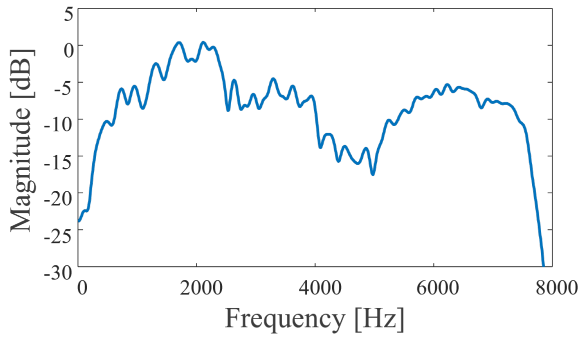

(a) Magnitude response.

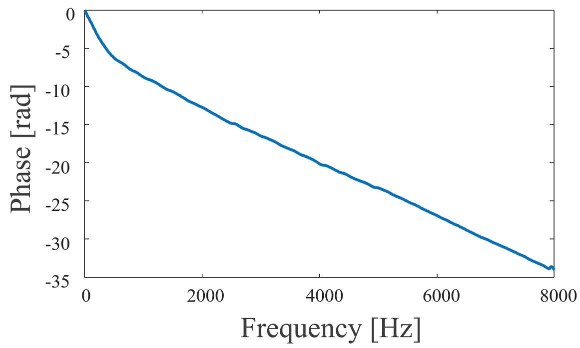

(b) Phase response.

Fig. 6: Frequency response of the secondary path.

Figure 9 displays the ANR curves for different algorithms, averaged over 100 trials. In this figure, black, yellow, red, blue lines represent the outcomes of TD-FxNLMS, TD-LFxNLMS, FD-FxNLMS, and FD-WFxNLMS algoritms, respectively. As can be seen from this figure, the performance of the FD-FxNLMS (the black line) matches that of the TD-FxNLMS (the red line) by adopting the step-size in Eq. (15). This figure cleary shows that the FD-WFxLMS algorithm achieves the fastest convergence. Particularly within the intervals of 2.5 s to 5 s and 7.5 s to 10 s, this algorithm excels in tracking the narrowband noise with time-varying

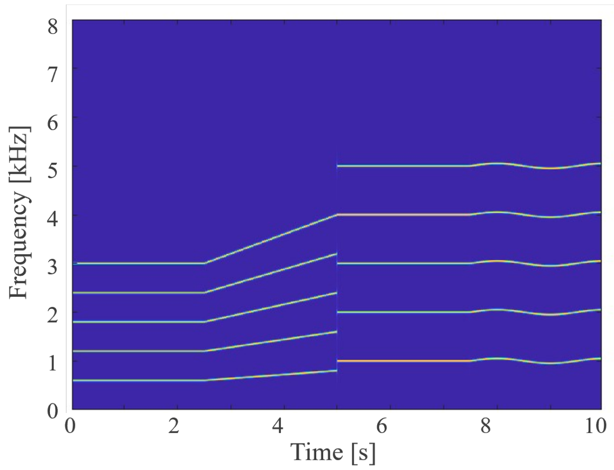

Fig. 7: Spectrogram of the narrowband noise in Case-I.

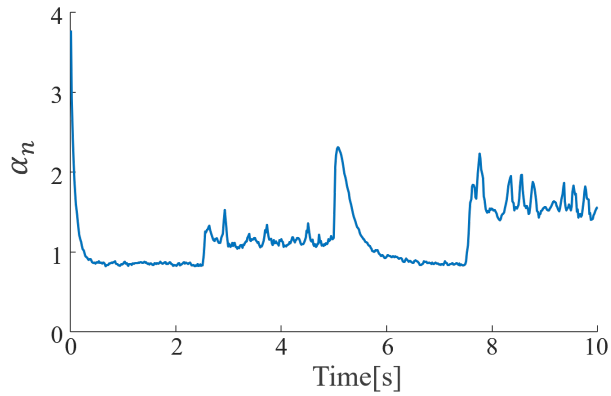

Fig. 8: Transient behavior of α_n in Case-I.

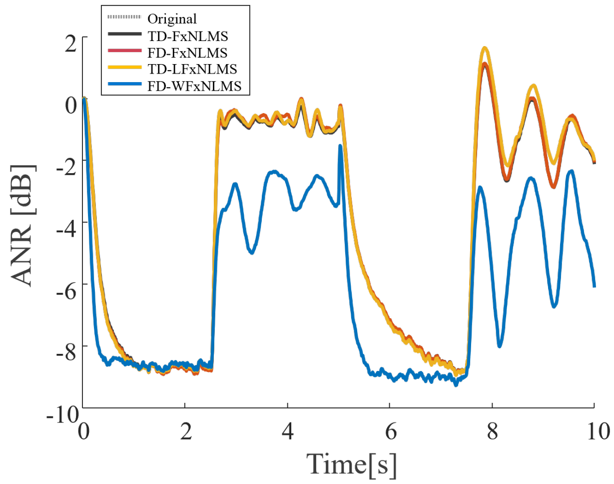

Fig. 9: ANC curves for various algorithms in Case-I (black: TD-FxNLMS, red: FD-FxNLMS, yellow: TD-LFxNLMS, blue: FD-WFxNLMS).

frequencies. Figure 10 illustrates the amplitude-frequency characteristics of output for each algorithm at 7 s. It is clear from this figure that the FD-FxWNLMS algorithm offers superior noise attenuation performance, particularly at 5 kHz

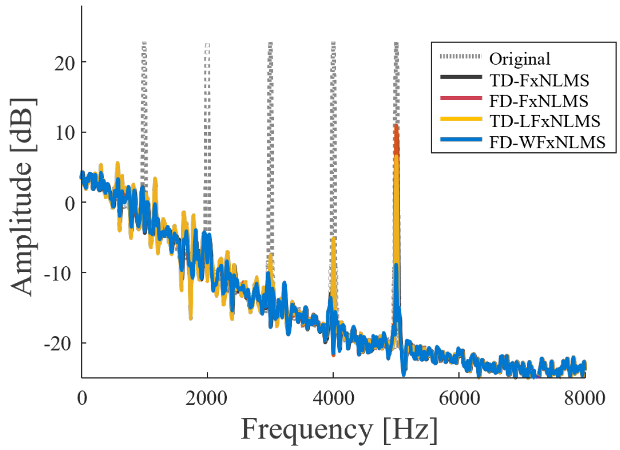

Fig. 10: Amplitude-frequency characteristics of output at 7.0 s for each algorithm in Case-I (gray: error signal, black: TD-FxNLMS, red: FD-FxNLMS, yellow: TD-LFxNLMS, blue: FD-WFxNLMS).

by at least 7 dB over other algorithms.

5.2 Case II: Active noise control using real noise

In the second experiment, we evaluate the convergence performance against real noise, specifically using vacuum cleaner noise [24]. Suppressing the narrowband signal generated by the motor of the vacuum cleaner is challenging because it varies over time according to electrical load of the motor. Additionally, the broadband noise produced by the exhaust further complicates the noise control process. The spectrogram of noise is depicted in Figure 11. In this noise, low-frequency peaks are predominantly found below 500 Hz, whereas high-frequency peaks, with a fundamental frequency oscillating around a central point of 2, 5 kHz, appear.

The transient behavior of α_n resulting from this experiment is shown in Figure 12. Although small frequency fluctuations are present in the noise after 1 s, α_n approximately converges to 1.

Figure 13 shows ANR curves for various algorithms. As shown in this figure, the performance of each algorithm is nearly identical. This is because each algorithm primarily focuses on controlling the low-frequency narrowband noise ($\sim$ 600 Hz), which has relatively large amplitude. Since the frequency fluctuations of this low-frequency noise are small, the impact of fast tracking ability of the proposed method is limited. However, at the points where the amplitude of this low-frequency noise changes (around 1.5 s and 2.5 s), the proposed method adapts more quickly to these changes and then achieves a lower ANR.

Figure 14 illustrates the amplitude-frequency characteristics of output for each algorithm at 7.0 s. This figure highlights that the FD-WFxNLMS algorithm exhibits superior control performance, achieving notable improvements of 5 dB at 100 Hz and 3 dB at 2.5 kHz.

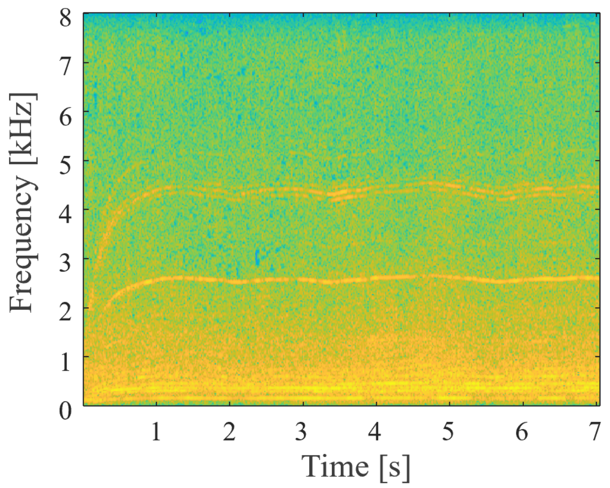

Fig. 11: Spectrogram of vacuum cleaner noise in Case-II.

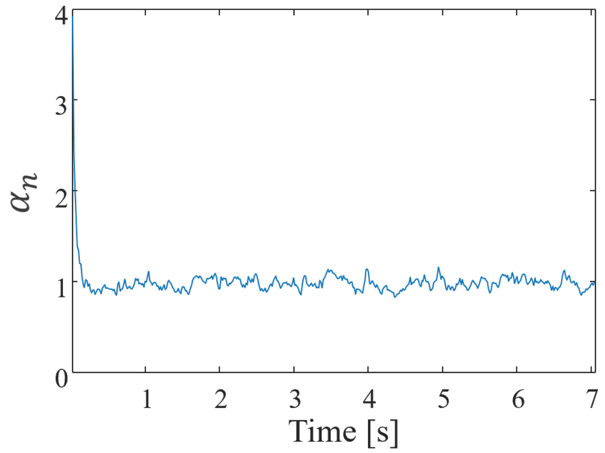

Fig. 12: Transient behavior of α_n in Case-II.

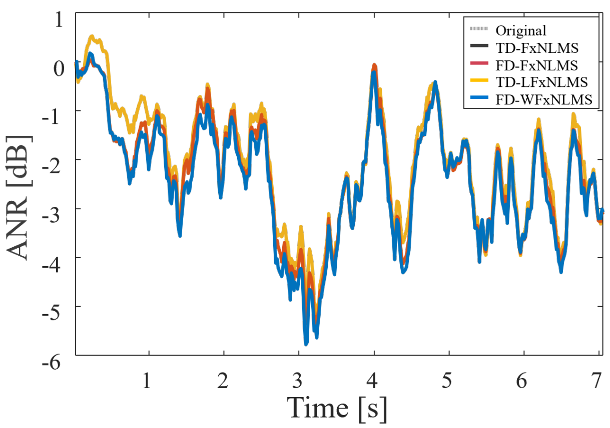

Fig. 13: ANC curves for various algorithms in Case-II (black: TD-FxNLMS, red: FD-FxNLMS, yellow: TD-LFxNLMS, blue: FD-WFxNLMS).

These experiments reveal that the FD-WFxNLMS algorithm provides fast convergence, thereby enhancing tracking performance for time-varying narrowband noise compared

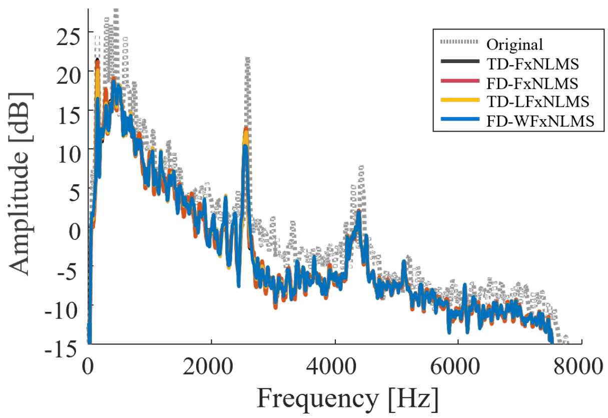

Fig. 14: Amplitude-frequency characteristics of output at 7.0 s for each algorithm in Case-II (gray: error signal, black: TD-NFxNLMS, red: FD-FxNLMS, yellow: TD-LFxNLMS, blue: FD-WFxNLMS).

to other conventional algorithms.

6. Conclusion

In this paper, we have proposed the frequency-domain weighted FxLMS algorithm for feedback active noise control in order to achieve the fast convergence. This method dynamically adjusts weights based on the amplitude-frequency characteristics of narrowband noise, thereby improving tracking performance for time-varying narrowband noise. Simulation experiments demonstrated that the FD-WFxNLMS algorithm secures fast convergence, surpassing traditional algorithms in feedback ANC settings.

The variable step-size (VSS) approach with frequency weighting is potentially applicable to both FxAP and FxRLS algorithms. FxAP, due to its similarity to FxNLMS, is expected to benefit directly from the VSS of the proposed method. In the case of FxRLS, it may be possible to assign more appropriate gain vectors or forgetting factors for each frequency. However, several challenges remain, such as the lack of an established method for efficiently computing FxRLS in the frequency domain.

References

[1] T. Schumacher, H. Krüger, M. Jeub, P. Vary, and C. Beaugeant,"Active noise control in headsets: A new approach for broadband feedback ANC," Proc. of 2011 IEEE International conference on acoustics, speech and signal processing (ICASSP), Prague, Czech Republic, pp. 417–420, 2011.

[2] S. M. Kuo, X. Kong, and W. S. Gan, "Applications of adaptive feedback active noise control system," IEEE Trans. Control Syst. Technol., 2003, Vo. 11, No. 2, pp. 216–220, Mar. 2003.

[3] M. Rupp and A. H. Sayed, "Modified FxLMS algorithms with improved convergence performance," Conference Record of The Twenty-Ninth Asilomar Conference on Signals, Systems and Computers, CA, USA, Vol. 2, pp. 1255–1259, 1995.

[4] S. Narasimhan, S. Veena, and H. Lokesha, "Variable step-size Griffiths' algorithm for improved performance of feedforward/feedback active noise control," Signal Image Video Process., Vol. 4, No. 3, pp.

309-–317, 2009.
[5] M. T. Akhtar , "Narrowband feedback active noise control systems with secondary path modeling using gain-controlled additive random noise," Digit. Signal Process., Vol. 111, No. 102976, pp. 1–13, 2021.
[6] S. Park, E. Patterson, and C. Baum, "Long short-term memory and convolutional neural networks for active noise control," Proc. 2019 5th International Conference on Frontiers of Signal Processing (ICFSP), Marseille, France, pp. 121-125, 2019.
[7] Y. J. Cha, A. Mostafavi, and S. S. Benipal, "DNoiseNet: Deep learning-based feedback active noise control in various noisy environments," Engineering Applications of Artificial Intelligence, Vol. 121, No. 105971, pp. 1–14, May 2023.
[8] Y. Tang, H. Zhang, and Y. Zhang, "Stability guaranteed active noise control: Algorithms and applications," IEEE Trans. Control Syst. Technol., Vol. 31, No. 4, pp. 1720–1732, July 2023.
[9] K. Gomathi, V. Saravanan, and N. S. kumari, "Variable step size for improving convergence of FxLMS algorithm," Procedia Technology, Vol. 25, pp. 420–426, 2016.
[10] Y. Jiang, S. Chen, H. Meng, Z. Zhou, and W. Lu, "A novel adaptive step-size hybrid active noise control system," Appl. Acoust., Vol. 182, No. 108285, pp. 1–14, 2021.
[11] L. Lu and H. Zhao, "Improved filtered-x least mean kurtosis algorithm for active noise control," Circuits Syst. Signal Process., Vol. 36, No. 4, pp. 1586—1603, 2017.
[12] A .M. A. Omour, A. Zidouri, N. Iqbal, and A. Zerguine, "Filtered-X least mean fourth (FXLMF) and leaky FXLMF adaptive algorithms," EURASIP J. Adv. Signal Process., Vol. 2016, No. 39, pp. 1–20, Apr. 2016.
[13] O. J. Tobias and R. Seara, "Leaky-FXLMS algorithm: stochastic analysis for Gaussian data and secondary path modeling error," IEEE Trans. Speech and Audio Process., Vol. 13, No. 6, pp. 1217–1230, Nov. 2005.
[14] L. Wu, X. Qiu, Y. Guo, "A generalized leaky FxLMS algorithm for tuning the waterbed effect of feedback active noise control systems," Mech. Syst. Signal Process., Vol. 106, pp. 13–23, Nov. 2018.
[15] C. Zhou, H. Zou, X. Qiu, "A frequency band constrained filtered–x least mean square algorithm for feedback active control systems," J. Acoust. Soc. Am., Vol. 148, No. 4, pp. 1947–1951, Oct. 2020.
[16] M. T. Akhtar and W. Mitsuhashi, "A modified normalized FxLMS algorithm for active control of impulsive noise," Proc. 2010 18th European Signal Processing Conference (EUSIPCO), Aalborg, Denmark, pp. 1–5, 2010.
[17] S. Zhang, Y. S. Wang, H. Guo, C. Yang, X. L. Wang, N. N. Liu, "A normalized frequency-domain block filtered-x LMS algorithm for active vehicle interior noise control," Mech. Syst. Signal Process., Vol. 120, No. 1, pp. 150—165, 2019.
[18] Z. Qiu, C.M. Lee, Z. H. Xu, and L. N. Sui, "A multi-resolution filtered-x LMS algorithm based on discrete wavelet transform for active noise control," Mech. Syst. Signal Process., Vol. 66–67, pp. 458–469, Jan. 2016.
[19] L. Luo, J. Sun, and B. Huang, "A novel feedback active noise control for broadband chaotic noise and random noise," Appl. Acoust., Vol. 16, No. C, pp. 229–237, Jan. 2017.
[20] V. Patel and J. Cheer, "A hybrid multi-reference subband control strategy for active noise control headphones," Appl. Acoust., Vol. 197, No. 108932, pp.1–13, Aug. 2022.
[21] ITU-T Recommendation G.191 (03/23), Software tools for speech and audio coding standardization, Mar. 2023.
[22] P. Song and H. Zhao "Filtered-x least mean square/fourth (FXLMS/F) algorithm for active noise control," Mech. Syst. Signal Process., Vol. 120, No. 1, pp. 69–82, Apr. 2019.
[23] A. Varga and H. J. Steeneken, "Assessment for automatic speech recognition: Ii. noisex-92: A database and an experiment to study the effect of additive noise on speech recognition systems," Speech Communication, Vol. 12, No. 3, pp. 247—251, Sep. 1993.
[24] R. Serizel, N. Turpault, A. P. Shah, and J. Salamon, "Sound event detection in synthetic domestic environments," Proc. 2020 IEEE International Conference on Acoustics, Speech and Signal Processing (ICASSP), Barcelona, Spain, pp. 86–90, 2020.

Appendix A: Derivatoin of Eq. (18)

The logarithmic function $\log_{10}(x)$ is monotonically increasing for $x > 0$. Therefore, the following property holds:

$$x < y \Rightarrow \log_{10}(x) < \log_{10}(y).$$

Hence, for the set $\boldsymbol{E}_k = \{|E_i|, i = l-k, \ldots, l+k\}$, the following holds:

$$E_p < E_q \Rightarrow \log_{10}(E_p) < \log_{10}(E_q),$$

where,

$$E_p \in \boldsymbol{E}_k, \quad \forall E_q \in \boldsymbol{E}_k \setminus \{E_p\}.$$

This means that if E_p is the minimum value of $\boldsymbol{E}_k$, then $\log_{10}(E_p)$ is also the minimum value of $\{\log_{10}|E_k|, i = l-k, \ldots, l+k\}$, i.e.,

$$\log_{10}(\Phi(E_k, l)) = \Phi(\log_{10}(E_k), l).$$

Then, Eq. (18) is derived.

Appendix B: Number of FFT-points

The time-domain FxLMS algorithm updates the k-th coefficient using the following equation:

$$w_k^{i+1} = w_k^i - \mu e_n \sum_{l=0}^{L-1} \hat{c}_l \hat{d}_{n-k-l}, \tag{A· 1}$$

where $k = 0, 2, \ldots, M-1$. This equation can be easily extended to the block FxLMS algorithm, which updates every K samples, as follows:

$$w_k^{i+1} = w_k^i - \mu \sum_{j=0}^{K-1} e_{n-j} \sum_{l=0}^{L-1} \hat{c}_l \hat{d}_{n-k-l-j}. \tag{A· 2}$$

Assuming L, K, and M are all less than or equal to N but close to N, this algorithm requires up to the past $3N$ samples of $\hat{d}_n$.

Given that N is represented as 2^k, $4N$-points FFT is necessary to compute the gradient term in the frequency domain. Since e_n has K points, c_n has L points, and d_n has $3N$ points, each signal is extended to $4N$ points using zero-padding before applying the FFT.

In feedforward ANC, the FD-FxLMS algorithm [17] simplifies computations by assuming d_n has only $2N$ points and applying a $2N$-points FFT. However, in feedback ANC, accumulated feedback errors significantly degrade convergence performance if d_n is not sufficiently long.

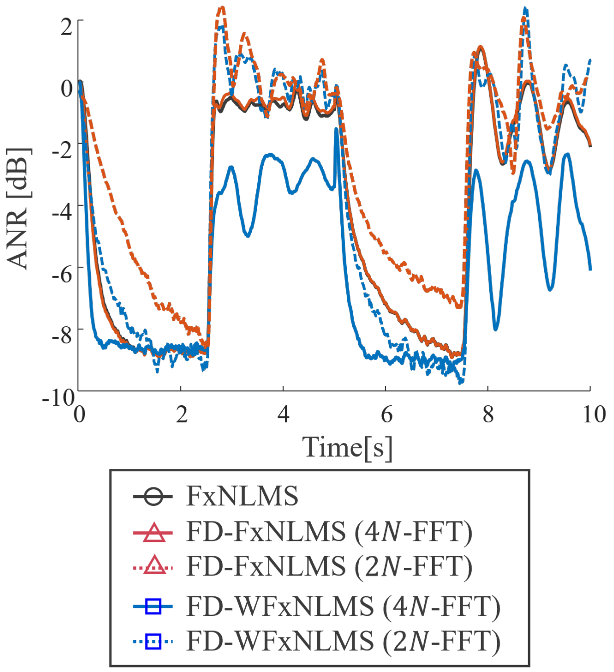

Fig. A· 1: Comparison of ANR (Active Noise Reduction) curves for algorithms using $2N$-point FFT and $4N$-point FFT.

Figure A· 1 compares the convergence performance of five algorithms: TD-FxNLMS, FD-FxNLMS with $2N$-points FFT, FD-FxNLMS with $4N$-points FFT, FD-WFxNLMS with $2N$-points FFT, and FD-WFxNLMS with $4N$-points FFT. The experimental conditions are identical to Case I in 5.1. As shown in the figure, the algorithms using $2N$-points FFT exhibit degraded convergence performance.

Yosuke Sugiura received his B.E., M.E., and Ph.D. degrees from Osaka University, Osaka, Japan in 2009, 2011, and 2013, respectively. In 2013, he joined the Tokyo University of Science, Tokyo, Japan. In 2015, he joined Saitama University, Saitama Japan, where he is currently an Assistant Professor. His research interests include digital signal processing, adaptive filter theory, and speech processing.

Ryota Noguchi received the B.E. degree from Saitama University, Saitama, Japan in 2023. He is currently a master's degree student at Saitama University. His research interests are in digital signal processing and adaptive filter theory.

Tetsuya Shimamura received his B.E., M.E., and Ph.D. degrees in electrical engineering from Keio University, Yokohama, Japan, in 1986, 1988, and 1991, respectively. In 1991, he joined Saitama University, Saitama, Japan, where he is currently a Professor. He was a visiting researcher at Loughborough University, UK in 1995 and at Queen ’ s University of Belfast, UK in 1996, respectively. Prof. Shimamura is an author and coauthor of six books. He serves as an editorial member of several international journals and is a member of the organizing and program committees of various international conferences. His research interests are in digital signal processing and its application to speech, image, and communication systems.